Chemi-ionization reactions involving metastable helium atoms at high energy

P. Pradel, J.J. Laucagne

J. Physique **44** (1983) 1263-1271 NOVEMBRE **1983,** PAGE 1263

Classification
Physics Abstracts
34.50

Chemi-ionization reactions involving metastable helium atoms at high energy

P. Pradel and J. J. Laucagne

Service de Physique des Atomes et des Surfaces, Centre d'Etudes Nucléaires de Saclay,
91191 Gif-sur-Yvette Cedex, France

(*Reçu le 2 mai 1983, révisé le 7 juillet, accepté le 28 juillet 1983*)

Résumé. — Nous avons utilisé un faisceau rapide d'atomes d'hélium métastable en collisions sur diverses cibles gazeuses, atomique (Ne) et moléculaires (H_2, N_2, O_2 et CO) afin d'étudier le comportement en fonction de l'énergie de la section efficace totale de chimie-ionisation de ces différents systèmes. Le domaine d'énergie étudié s'étend depuis le supra-thermique (15 eV) jusqu'aux énergies moyennes (1 500 eV). Les cibles moléculaires ont permis de distinguer l'ionisation simple et l'ionisation dissociative ; dans le premier cas, les résultats présentent une grande dépendance énergétique de la section efficace tandis que dans le second nous avons mis en évidence un seuil énergétique pour l'apparition de l'ion dissociatif, qui dépend du défaut d'énergie de la réaction.

Abstract. — Total chemi-ionization cross-sections have been measured over the 15 to 1 500 eV energy interval for collisions of He 2 ^{1}S and 2 ^{3}S metastable atoms with Ne, H_2, N_2, O_2 and CO, using a slow ion measurement technique. With molecular targets these measurements have shown a strong energy dependence for the total ionization cross-section without dissociation. In the case of dissociative ionization an energy threshold appears, dependent on the energy defect of the reaction.

1. Introduction.

Over the last decade the chemi-ionization of atomic or molecular gases by metastable helium impact has been studied extensively [1-6]. From a theoretical point of view chemi-ionization processes include two broad classes of reactions : collisions with removal of an electron (Penning ionization, associative ionization, dissociative ionization, rearrangement ionization) and collisions with formation of an ion pair. In the first class a transition to the continuum is involved and a new particle, the free electron is present in the exit channel. After a collision with ion pair formation, on the contrary, the number of particles remains unchanged in the exit channel and transitions occur between discrete levels of the electronic energy. Our work concerns electron removal processes and we are therefore dealing with a transition of quasimolecular systems to the continuum, for which the theory is incompletely developed.

Most experiments, using atomic targets, have measured the energy dependence of the total Penning ionization cross-section : at low energy the first data were reported by Tang *et al.* [1] for the systems Ne*/Ar, Kr and Xe, where Ne* represents the metastable states of Ne, and by Pesnelle *et al.* [2] for the He* + Ar system, He* being the metastable states of He. Later, the velocity dependence of the Penning and associative ionization cross-sections of Ar atoms by He (2 ^{3}S) and He (2 ^{1}S) metastable atoms have been measured in the 30-400 meV energy range, in a crossed-beam experiment using a time of flight technique, by Pesnelle *et al.* [3]. Illenberger and Niehaus [4] have measured the energy dependence of the total Penning ionization cross-section in the 20-400 meV energy range for the collision systems He (2 ^{3}S)/Ar, Kr, Xe, N_2, Hg, He (2 ^{1}S)/Ar, Kr, Xe, N_2, Hg.

The quenching rate of He (2 ^{3}S) by Ar has been measured by Lindinger *et al.* [5] in a flowing afterglow in the 300-900 K temperature range.

Some collision studies on excited particles at high energy ($E > 1$ keV) such as He (2 ^{1}S, 2 ^{3}S) and H (2 S) in collision with rares gases or molecules have been carried out to determine the electron capture, electron loss or collisional destruction cross-section of the excited species [6-8] ; in these experiments only the fast product of the reaction was measured.

Little has been done in the superthermal energy range (10-100 eV) because of the difficulty of producing and detecting the metastable atoms, though some scattering experiments have been carried out

with such metastable beams : Morgenstern *et al.* [9*a*] have studied the differential scattering cross-section of He ($2\ ^3S$) on He ($1\ ^1S$) at energies between 5 and 10 eV and Gillen *et al.* [9*b*] have performed differential cross-section measurements for He^+ production in the collision of He* ($2\ ^3S$ and $2\ ^1S$) with He at centre-of-mass energies of 50.99 eV and 199 eV. Moseley *et al.* [9*c*] have measured the deexcitation cross-section for mixed beams of He ($2\ ^3S$) and He ($2\ ^1S$) in N_2, Ar and C_2H_2 by collecting slow ions, in the 50 to 600 eV energy range.

The present work is devoted to relative cross-section measurements for the ionization of the atomic target Ne and the molecular targets H_2, N_2, O_2, CO by both He ($2\ ^1S$) and ($2\ ^3S$) in the laboratory energy range 15-1 500 eV, using a mass analysis technique in the detection of the slow ions created. For these molecular target gases the ionization potential of the target is a few eV lower than the excitation energy of the metastable He atom (see Table I). The initial state of the collision complex is embedded in a continuum and is subject to autoionization at small distances (Penning ionization). In the energy range covered we must consider the possibility of ion creation from an excitation transfer followed by autoionization of the target. This mechanism becomes more and more efficient with increasing collision energy and concerns both atomic and molecular targets [10]; the autoionization of the target can be extremely efficient, and under our experimental conditions we are not able to estimate its relative importance. These two processes are expected to be the predominant modes of slow ion production according to the following reactions.

1.1 FOR SYMMETRICAL DIATOMIC MOLECULES.

1.1.1 *Penning ionization process* (*total cross-section* σ_P).

$$He\,(2\ ^1S, 2\ ^3S) + X_2 \rightarrow (HeX_2)^* \rightarrow \rightarrow He\,(1\ ^1S) + X_2^+ + e^- \quad \Delta E > 0. \quad (1)$$

1.1.2 *Autoionization process* (*total cross-section* σ_A).

$$He\,(2\ ^1S, 2\ ^3S) + X_2 \rightarrow He\ 1\ ^1S + X_2^* \rightarrow \rightarrow He\ 1\ ^1S + X_2^+ + e^- \quad \Delta E > 0. \quad (2)$$

In this paper the ionization cross-sections corresponding to processes (1) and (2) will be written σ_{P+A}, such that :

$$\sigma_{P+A} = \sigma_P + \sigma_A. \quad (3)$$

1.1.3 *Dissociative ionization process* (*total cross-section* σ_D).

Under the same experimental conditions we have also measured the energy dependence of dissociative ionization of the molecular target gas. Locht *et al.* [11], Locht [12] and Dehmer and Chupka [13] have shown that the autoionizing levels may play a considerable part in the dissociation of molecular ions such as N_2^+ and O_2^+. This can be written :

$$He\,(2\ ^1S, 2\ ^3S) + X_2 \rightarrow He\,(1\ ^1S) + + X^+ + X + e^- \quad \Delta E. \quad (4)$$

The energy defect can be positive or negative depending on the target dissociation energy (see Table I). If negative, the defect energy is taken from the kinetic energy of the metastable atom.

1.2 FOR ASYMMETRICAL DIATOMIC MOLECULE (CO IN THIS CASE). — Reactions 1 and 2 (Penning ionization and autoionization processes) are the same if we replace X_2 by XY. For dissociative ionization however two processes are possible with different total dissociative ionization cross-sections σ_D :

$$He\,(2\ ^1S, 2\ ^3S) + XY \rightarrow \rightarrow He\,(1\ ^1S) + X^+ + Y + e^- \quad \Delta E \quad (5)$$

and

$$He\,(2\ ^1S, 2\ ^3S) + XY \rightarrow \rightarrow He\,(1\ ^1S) + X + Y^+ + e^- \quad \Delta E. \quad (6)$$

Table I. — *Ionization potential, dissociation energy and energy defect for the different processes and targets studied in this experiment.*

Substance	Ionization potential	Dissociation energy	ΔE (eV) Penning ionization		ΔE (eV) Dissociative ionization	
			$2\ ^3S$	$2\ ^1S$	$2\ ^3S$	$2\ ^1S$
Ne	21.56		− 1.76	− 0.96		
Ar	15.75		4.04	4.84		
H_2	15.43	4.48	4.37	5.17	1.77	2.57
N_2	15.57	9.76	4.12	4.92	− 4.47	− 3.67
O_2	12.06	5.08	7.74	8.54	1.8	1.88
CO	14.01	11.11	5.79	6.59	− 5.11 ; − 2.71 (O^+) (C^+)	− 4.31 ; − 1.91 (O^+) (C^+)

For this target (CO) the energy defects ΔE of reactions 5 and 6 are negative (see Table I).

We also present in this work a comparison between an endothermal reaction involving Ne target atoms such as :

$$He(2\,^1S, 2\,^3S) + Ne \rightarrow \rightarrow He(1\,^1S) + Ne^+ + e^- \quad \Delta E < 0 \quad (7)$$

and an exothermal reaction involving Ar target atoms :

$$He(2\,^1S, 2\,^3S) + Ar \rightarrow \rightarrow He(1\,^1S) + Ar^+ + e^- \quad \Delta E > 0\,. \quad (8)$$

The latter reaction has already been investigated under the same experimental conditions [14]. Owing to the negative energy defect of the reaction 7 a kinetic energy threshold is expected to be observed in the production of Ne^+ ions, while reaction 8, with positive energy defect, exhibits no threshold in our energy range.

2. Apparatus.

2.1 GENERAL DESCRIPTION. — A schematic view of the apparatus is shown in figure 1.

The first part of the set-up is essentially the same as that used in our studies of differential cross-sections for elastic and inelastic scattering of the H^+Cs and HCs systems [15] and hence will only be recalled briefly here. A 500 eV He^+ beam is produced by a water-cooled Colutron source, model 100, working with a hot cathode positive ion glow discharge. The ion beam is extracted through a molybdenum anode hole 0.5 mm in diameter and accelerated by a negatively biased electrode, which is also the first electrode of the cylindrical lens. After focusing, the He^+ beam is decelerated by a Menzinger retardation system model 400 from 500 eV to the working energy when the latter is less than 300 eV. For energies above 300 eV the ion beam is extracted directly from the source at working energy.

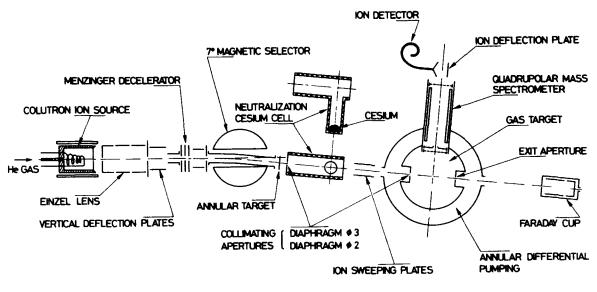

Fig. 1. — Schematic diagram of the apparatus. The drawing is not to scale. For clarity the neutralization caesium cell is shown from the top. The annular target is located in front of the collimating apertures.

In order to eliminate the fast neutral beam resulting from charge exchange with the residual gas in the region near the ion source (see Fig. 1) the first section of the apparatus, including the ion source, focalization lens and Menzinger decelerator, was de-aligned by rotation in the horizontal plane. By means of a 7° magnetic selector the He^+ beam is deflected and adjusted on the geometrical axis of the neutralization cell. These fast neutrals are mainly produced by the resonant reaction :

$$He^+ + He \rightarrow He + He^+ \quad (9)$$

which is efficient in the region located between the anode and the decelerator, where the background He pressure is of the order of 10^{-5} torr.

The He^+ beam enters the neutralization caesium cell where it is partly converted into He atoms in metastable states by charge exchange collisions. Neutralization occurs from the quasi-resonant reactions [16-18] :

$$He^+ + Cs \rightarrow He(2\,^3S) + Cs^+ \quad \Delta E = 0.91\,eV \quad (10)$$

$$He^+ + Cs \rightarrow He(2\,^1S) + Cs^+ \quad \Delta E = 0.12\,eV\,. \quad (11)$$

The small energy defect results in a large cross-section for these collisions at low energy and provides a means of obtaining intense He ($2\,^3S$) and He ($2\,^1S$) beams [19]. The neutralization caesium cell has been described in detail elsewhere [15] and is only recalled briefly here. It consists of a horizontal pure copper tube limited by entrance and exit diaphragms, 3 mm in diameter; the entrance aperture acts as a first collimating diaphragm. Its boiler is a cylinder with its axis perpendicular to the beam axis (see Fig. 1) containing approximately 4 g of caesium.

After passage through the neutralization cell the neutral beam consists of helium atoms in :

i) the metastable triplet $2\,^3S$ state (produced by deexcitation of the $2\,^3P$ state [18]),

ii) the metastable singlet $2\,^1S$ state (directly excited),

iii) the $1\,^1S$ ground state (due mainly to deexcitation of the $2\,^1P$ state).

The relative abundances of these three components were not measured in the present experiment, but from the data obtained by Reynaud *et al.* [18] with a Cs cell the composition of the emerging helium neutral beam is well known in the 100-1 000 eV range (see Table II). For energies below 100 eV two procedures may be used to estimate the composition of the metastable He beam with reasonable confidence.

In our previous work [14] the cross-section for Penning ionization of Ar in collisions with metastable He atoms was measured in the energy range 12-1 500 eV and compared with theoretical predictions on the triplet $2\,^3S$ and singlet $2\,^1S$ metastable states of He (curves A and B of Fig. 2 in Ref. 14). Metastable He atoms were also produced by charge exchange of

Table II. — He ($2\,^3S$) *and* He ($2\,^1S$) *relative abundances in the neutral emerging beam according to reference* 18.

E (eV)	12	50	100	150	200	300	500	750	1 000
$2\,^3S$ %	25 (a)	35 (a)	46	49	59	67	73	72	72
$2\,^1S$ %	75 (a)	65 (a)	54	51	41	33	27	28	28

(a) Values estimated from reference 14 and from extrapolation of the data in reference 18.

He^+ ions in Cs vapour under the same conditions as in the present experiment. At 100 eV the data of reference 14 correspond to a neutral beam composed of about 50 % $2\,^1S$ states and 50 % $2\,^3S$ states in close agreement with the measurements of Reynaud *et al.* (46 % $2\,^1S$ states and 54 % $2\,^3S$ states). As the energy decreases below 100 eV the experimental points of reference 14 approach the theoretical curve B of the $2\,^1S$ state, showing that the relative abundance of singlet $2\,^1S$ metastable He atoms increases in the neutral beam at energies lower than 100 eV. An estimate of the neutral beam composition at 12 eV leads to 75 % $2\,^1S$ states and 25 % $2\,^3S$ states. An extrapolation of the data of Reynaud *et al.* towards the low energy range gives the same composition of the neutral beam at 12 eV. The composition of the neutral He beam according to these procedures is given in table II.

Concerning the He ($1\,^1S$) neutral beam composition this state comes from radiative deexcitation of the He ($2\,^1P$) state which is not greatly excited; an upper limit of 10 % can be estimated with reasonable confidence [18].

At the neutralization caesium cell exit the remaining He^+ and newly formed He^- ions are swept away by a weak transverse electric field (100 $V.cm^{-1}$) applied between two cylindrical plates 42 mm long, 15 mm in diameter and 3 mm apart. The neutral beam then enters the gas-target collision chamber; this interaction chamber is a small cylindrical box, 16 mm in diameter, with two apertures for passage of the beam through the target. The 2 mm diameter entrance aperture is the second collimating diaphragm and the exit aperture, 2.6 mm in diameter, permits an angular divergence of 1°. The different target gases studied are introduced into the collision chamber through a leak valve and their pressure is monitored by a Westinghouse ionization gauge. The target gas pressure is adjusted to maintain single-collision conditions in the chamber, i.e. a linear dependence of the measured emerging ion signal against the gas pressure.

A differential pumping system keeps a background pressure of 1×10^{-7} torr in the assembly the total pumping capacity being approximately 4 000 $l.s^{-1}$.

2.2 SLOW ION DETECTION. — The slow target gas ions resulting from reactions [1-8] are extracted from the collision chamber, biased at approximately + 20 V relative to ground potential, through an aperture lying on an axis centred at the middle of the collision zone and perpendicular to the neutral beam axis (see Fig. 1). The ions are focused by an electrostatic lens consisting of the collision chamber, a 10 mm diameter grid biased at − 80 V and a 2 mm diameter grounded diaphragm. The ions are mass-selected by a RIBER quadrupole mass spectrometer and detected by an RTC channeltron, model B 419 BL-01, placed perpendicularly to the quadrupole axis so that photons emitted in the colliding zone are not seen by the channeltron which detects only the slow ions.

Our measurements are not absolute because :

i) the quadrupole mass analyser efficiency is not known, and

ii) the measurement of the targets gas pressures are not absolute : our Westinghouse gauge only monitore the gas pressure.

It was verified that an electric field of 80 $V.cm^{-1}$ (corresponding to the bias values of the collision chamber and grid mentioned above) ensured saturation of the thermal ion signal for all the projectile velocities in our energy range. The detection efficiency is found to be independent of the He* energy, showing that a negligible kinetic energy is transferred to the Penning ions.

Besides the thermal ions it is well known that dissociative ions may have initial kinetic energies of a few eV in excess of the thermal energy and over a wide azimuthal angle range [20], because these ions often come from highly excited dissociative states of the molecular ion. The population of these states grows as the He* kinetic energy increases, so more and more dissociative ions will appear with high kinetic energy. Since it was not technically possible to increase the extraction electric field far beyond 100 $V.cm^{-1}$ the detection efficiency g for these ions remains below 1; its value is probably close to unity in the neighbourhood of the threshold then decreases with rising He metastable kinetic energy. Since the saturated dissociative ion signal is believed not to be reached in this experiment it is not possible to compare directly the thermal ion flux resulting from Penning ionization of the gas target and the ion flux resulting from dissociative ionization of the same target. Our measurements on the dissociative ion cross-section σ_D thus constitute a lower limit for the cross-section of the dissociative ionization process; however this experiment gives the threshold of the process with good accuracy.

Pulses resulting from ion impact at the channeltron were amplified then accumulated in a counting scale over a preselected time interval and the data were printed out on a teletype. The quadrupole spectrometer was adjusted on the chosen mass of the spectrum and the maximum of the corresponding peak was scanned by d.c. voltage sweeping on the quadrupole

at a frequency of approximately 60 Hz to prevent slight mass analyser variations. An electron gun (not shown in Fig. 1) located perpendicularly to both the quadrupole mass spectrometer axis and the neutral beam axis is used to test the mass scale of the quadrupole analyser and to identify the target ions without the neutral beam. After the gas cell, on the neutral beam axis, a stainless steel Faraday cup with secondary electron suppressor enables the He^+ beam to be both set and measured; the metastable beam was also detected from this stainless steel target by Auger electron emission, the cylindrical suppressor bias being inverted to attract secondary electrons in order to measure the product :

$$N'^* = N^* \gamma^* \tag{12}$$

where N^* is the metastable atom flux leaving the collision chamber and γ^* the secondary electron ejection coefficient of the metastable atom. Typically a + 20 V draw-out potential difference between the target and the suppressor cylinder was used; the positive current to the target was measured by a KEITHLEY 610 C electrometer using an input resistance of 10^{14} Ω.

3. Experimental procedure.

3.1 Determination of cross-sections σ_{P+A} and σ_D. — The slow-ion measurement method is applicable in cases where slow ions are produced in abundance by the excited beam, such as in Penning ionization collision. Consequently it is possible to work with a very low gas target pressure ensuring little attenuation of the neutral beam. Typically we have $\sigma n l \approx 10^{-3}$ (single-collision condition) where σ is the total inelastic cross-section, n the target density and l the effective target length; however these slow ion measurements fail to distinguish between different metastable states in a mixed beam. From the quasi-resonant reactions 10 and 11 at the neutralization cell exit the neutral mixed He ($2\,^1S$) and He ($2\,^3S$) beam flux is such that

$$N^* = N_0^+ \sigma_{+0} \pi_{Cs} \tag{13}$$

where $\pi_{Cs} = n_{Cs} \times L$ is the effective neutralization target thickness (n_{Cs} being the caesium density and L the effective caesium target length), σ_{+0} the total charge exchange cross-section for the formation of all neutral states of helium, N_0^+ the initial He^+ beam flux and N^* the total metastable atom beam flux.

For a given energy let N^* be the metastable atom flux entering the collision chamber $N_{X_2}^+$, the X_2^+ slow-ion flux entering the quadrupole created from reactions 1, 2 or 7, 8, is related to the σ_{P+A} ionization cross-section by :

$$N_{X_2}^+ = f N^* \sigma_{P+A} n_{X_2} l \tag{14}$$

where σ_{P+A} is expressed in cm^2, $f = 1$ for thermal ions, n_{X_2} is the target gas density (particles cm^{-3}) and l the effective gas target cell length (cm).

In the same way N_X^+, the X^+ slow-ion flux from dissociative ionization (reactions 4, 5, 6), will be equal to :

$$N_X^+ = g N^* \sigma_D n_{X_2} l \tag{15}$$

where $g < 1$ is the detection efficiency and σ_D is expressed in cm^2. Ionization caused by ground state atoms present in the beam is assumed to be negligible. This is justified because the corresponding cross-sections are lower by an order of magnitude than the observed cross-section σ_{P+A}, σ_D [9c] and the ground state atom flux does not exceed 0.1 N^* (see § 2.1).

3.2 Determination of γ^*. — Although the measured cross-sections are relative the secondary electron ejection coefficient of the metastable atom must be known, γ^* being a function of the metastable beam energy.

Equation 12 shows that the N^* metastable flux is obtainable from the product $N^* \gamma^*$ given by the Faraday cup so it is necessary to know γ^* in this energy range. The Faraday cup has an alkaline-contaminated stainless steel surface as a caesium flux from the caesium neutralization cell reaches and covers it (see Fig. 1). From the work of Hagstrum [21] it is well known that the work function $W\varphi$ of a metallic surface can be reduced by alkaline contamination. For instance $W\varphi = 1.6$ eV in the case of potassium on nickel. In this case Hagstrum has demonstrated experimentally that near the surface a low-energy incident ion is resonantly neutralized to an excited atom which is rapidly deexcited with the ejection of an Auger electron; hence the slow ion secondary emission process near a metal surface of sufficiently small work function $W\varphi$ is quite similar to that of a metastable atom. In our experiment it is reasonable to assume that the work function of the Faraday cup surface is lower than 2 eV and it is therefore possible at low energy to take as a good approximation γ^+ (the secondary emission coefficient for He^+) equal to γ^*. For high-energy incident He^+ ions ($E > 500$ eV) scattering effects become negligible so we may calculate γ^* directly knowing N^+, the remaining He^+ flux reaching the Faraday cup without target gas in the collision chamber :

$$N^+ = N_0^+ e^{-\sigma_{+0}\pi_{Cs}}. \tag{16}$$

The true value of N^* may be calculated from (13) and (16) :

$$N^* = N^+ e^{+\sigma_{+0}\pi_{Cs}} \sigma_{+0} \pi_{Cs}. \tag{17}$$

On the other hand $N'^* = N^* \gamma^*$ can be obtained directly from the Faraday cup (see section 2). Knowing the total exchange cross-section σ_{+0} for the formation

of all neutral states of helium [19] and the caesium cell temperature which gives π_{Cs} [22, 23] we can deduce N^* from equation 17 and γ^* from 12. The He^+ secondary emission coefficient γ^+ can be obtained from a well known Faraday cup measurement procedure where the cylindrical suppressor bias is inverted (see Fig. 2). If we compare the γ^* and γ^+ values independently determined in the energy range 500-1 500 eV we find that γ^+ is equal to γ^* within 5 % uncertainty. In conclusion we shall take $\gamma^* = \gamma^+$ throughout our experimental energy range (see Fig. 2) and assume from equations 12, 14 and 15 that the σ_{P+A} and σ_D ionization cross-sections of the target gas, studied here by He*, can be approximated by :

$$\sigma_{P+A} \approx N^+_{X_2}\, \gamma^+ / N'^* \, n_{X_2}\, lf$$

and

$$\sigma_D \approx N^+_X\, \gamma^+ / N'^* \, n_{X_2}\, lg\,. \qquad (18)$$

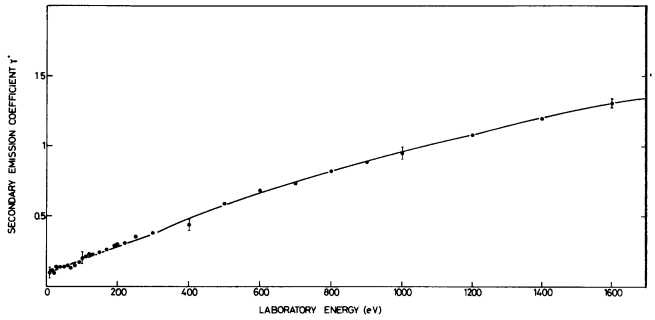

Fig. 2. — Secondary emission coefficient γ^+ for He^+ ions on a caesium contaminated stainless steel surface at normal incidence. γ^+ is obtained from three measurements : i) without ion deviation, cylindrical suppressor bias voltage negative relative to the target : yield I_1 ; ii) without ion deviation, cylindrical suppressor bias voltage positive : yield I_2 ; iii) with ion deviation out of the beam and cylindrical suppressor bias voltage positive : yield I_3. A straightforward analysis gives :

$$1 + \gamma^+ = (I_2 - I_3)/I_1\,.$$

4. Results.

4.1 ATOMIC TARGET CASE. — The experimentally determined Penning ionization cross-section σ_{P+A} of Ar on impact by He* atoms is plotted against the laboratory energy in figure 3*a*. These results, taken from our previous letter [14], are normalized to the absolute values of Moseley *et al.* at 100 eV [9*c*]. In their discussion the authors concluded that Penning ionization is expected to be the dominant process for slow ion production. Our relative cross-section σ_{P+A} is in good agreement with their experimental data, but in neither experiment is it possible to determine the ion fraction created from the autoionization process (see section 1). In the same energy range we present in figure 3*b* our measurements of the total

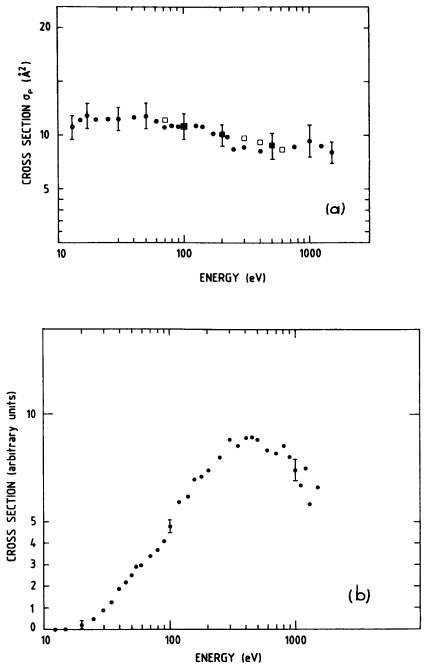

Fig. 3. — Comparison of experimental results for both Ar (exothermal case) and Ne (endothermal case) targets colliding with He*. 3*a*. — Ar slow ion data taken from our previous letter [14]. These results (closed circles) are normalized to the absolute values of references [9*c*] (open square). This cross-section shows a slight variation from 12 to 1 500 eV. 3*b*. — Total ionization cross-section of Ne in the same energy range as Ar, showing the strong energy dependence of the cross-section in this energy range.

ionization cross-section for Ne in collisions with He* atoms. For this system no previous absolute data are available so the present results are relative. If we compare the ionization of Ar (exothermal case, reaction 8) and Ne (endothermal case, reaction 7) targets the kinetic energy dependence of the cross-section σ_{P+A} appears to be quite different.

For an Ar target σ_{P+A} decreases slowly with increasing energy from 11 Å^2 at 13 eV to 8 Å^2 at 1 500 eV, whereas in the case of an Ne target the Ne^+ ion flux exhibits a threshold in the vicinity of 20 eV then rises rapidly with increasing energy to a sharp maximum near 400 eV. The Penning ionization process in Ne is endothermal by 1.76 eV and 0.96 eV respectively for He ($2\,^3S$) and He ($2\,^1S$) projectiles. Figure 3*b* shows that a relative kinetic energy as high as 16 eV, in the centre-of-mass coordinates, is needed to transfer about 1 or 2 eV to the internal energy of the colliding system. The cross-section for an Ne target decreases rapidly beyond 400 eV in the third part of the energy range, owing to the high relative velocity of the reactants.

4.2 MOLECULAR TARGET CASE.

4.2.1 *Molecular nitrogen.* — The total ionization cross-sections σ_{P+A} and σ_D for N_2 in collisions with He* are shown in figure 4. The open circles represent

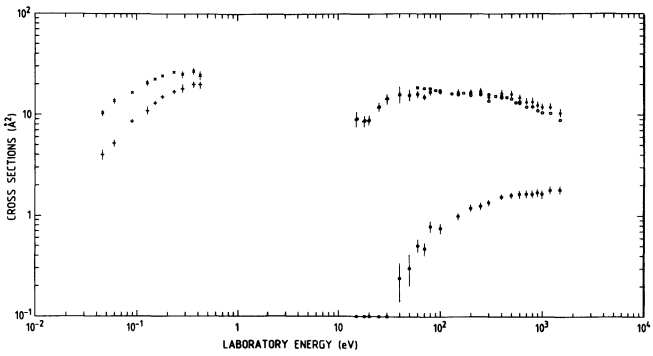

Fig. 4. — Energy dependence of the total ionization cross-section σ_{P+A} for the He^*/N_2 system is represented by open circles, that of the total dissociation ionization cross-section σ_D by closed circles. Closed triangles refer to the sum $\sum_i \sigma_i = \sigma_{P+A} + \sigma_D$ for comparison with the absolute slow ion measurements of Moseley *et al.* [9*c*] represented by open squares; the present data are normalized to the 100 eV point of reference 9*c*. Comparisons are also given with the absolute results of Illenberger and Niehaus [4] in the thermal energy range : (× × ×) for the He ($2\,^1S$)/N_2 system and (+ + +) for He ($2\,^3S$)/N_2.

the total Penning and autoionization cross-section σ_{P+A}, the closed circles the total dissociative ionization cross-section σ_D (endothermal case) and the closed triangles the sum $\sum_i \sigma_i = \sigma_{P+A} + \sigma_D$, which is compared with previous absolute slow ion measurements from Moseley *et al.* [9*c*] (open squares). The error bars include statistical uncertainty on the data. σ_D is determined from the dissociative ion flux measured with a detection efficiency lower than for σ_{P+A} (see section 2.2), but σ_D is more than one order of magnitude smaller than σ_{P+A} so it is possible to sum $\sigma_{P+A} + \sigma_D$ within a reasonable uncertainty. Our experimental points cover the range 15-1 500 eV and are normalized to the absolute values of Moseley *et al.* [9*c*] (100 eV being the normalized point). The kinetic energy dependence of our total cross-section agrees well with that of reference [9*c*] in the common energy range (60-600 eV) within the limits of uncertainty (± 15 %). As the energy increases from 15 to 100 eV σ_{P+A} rises towards a smooth maximum then decreases : the efficiency of the collision for these channels diminishes with increasing relative velocity. The total dissociative ionization cross-section for the system $He^* + N_2$ presents a threshold at approximately 40 eV (endothermal reaction, see Table I) above which it increases with energy, showing no structure in our energy range.

In the thermal energy range Illenberger and Niehaus [4] have studied the relative velocity dependence of the total Penning ionization cross-section for the He^*/N_2 system. The authors give relative data normalized to the absolute destruction rate constants obtained by the flowing afterglow technique at 300 K [28]. Their results (see Fig. 4) show a strong velocity dependence : the cross-section increases with collision energy to reach the values 25 Å² and 20 Å² for the $2\,^1S/N_2$ and $2\,^3S/N_2$ systems respectively, corresponding to the maximum relative collision energy of 0.4 eV.

Figure 4 gives the Penning ionization cross-section from reference 4 by comparison with the present total cross-section σ_{P+A}. The general behaviour the two sets of data is found to be quite coherent, especially if the present results (obtained with 75 % He ($2\,^1S$) at 12 eV, see section 2.1) are compared with the ($2\,^1S$)/N_2 cross-section of reference 4. In view of the large energy range covered by these data (5 decades), it would be very interesting to have a theroretical interpretation of the chemi-ionization process in N_2 from the thermal to the high energy range.

4.2.2 *Molecular hydrogen.* — The simplest case involving a molecular target is the chemi-ionization of H_2 by He*. This system has been studied theoretically by Cohen and Lane [24], who calculated the total chemi-ionization cross-section in terms of a local complex potential using either the spherical-potential approximation or sudden approximations at energies below 10 eV. Hickman *et al.* [25] have shown, from a theoretical study on the Penning ionization of H_2 by He* in the energy range 0.010-0.5 eV, that the total ionization cross-section increases sharply with energy. Earlier experimental work on the chemi-ionization of H_2 by He metastable atoms was carried out by Hotop and Niehaus [26] who measured the electron energy spectra arising from He ($2\,^3S$)-H_2 collisions. Neynaber *et al.* [27] have used merging beams to measure the absolute cross-section in the associative ionization process for a mixed metastable beam in the 0.01 to 0.8 eV energy range. Lindinger *et al.* [5] have measured the reaction rate constant for the quenching of the $2\,^3S$ state of He by H_2 as a function of temperature between 300 and 900 K : the measurements show that the rate constant increases rapidly with temperature.

Since the total chemi-ionization cross-section varies rapidly with energy in the thermal range it was not possible to normalize our relative data with reasonable confidence. Extrapolation of the present data to the thermal energy range would be meaningless. The theoretical calculations of Cohen and Lane [24] give a total chemi-ionization cross-section value of 18.5 Å² for 10 eV relative collision energy (averaged value for the singlet and triplet states).

Because the excitation energy of He* is high the electronic energy of $He^* + H_2$ exceeds that of the $He + H_2^+ + e^-$ (Penning ionization) and $He + H(1s) + H^+ + e^-$ (dissociative ionization) as shown in table I. The quasimolecule $He^* + H_2$ is therefore unstable with respect to autoionization at all interatomic separations, hence the processes $He^* + H_2 \rightarrow He + H_2^+ + e^-$ and $He^* + H_2 \rightarrow He + H^+ + H(1s) + e^-$ are exothermal. We note that in our energy range the formation of associative ions

such as HeH_2^+ is impossible due to the high relative velocity of the colliding partners. The present results for a molecular hydrogen target colliding with He* atoms are shown in figure 5. Both experimental total ionization cross-sections σ_{P+A} and σ_D are plotted against the laboratory energy. σ_{P+A} (open circles) increases sharply from 15 to 30 eV, then flattens out with a slight maximum at 200 eV and drops quickly after 1 keV because of the magnitude of the relative velocity. σ_D behaves differently : above 15 eV this value (closed circles) rises slowly to reach a maximum in the neighbourhood of 150 eV, then falls slightly and remain constant up to our maximum energy.

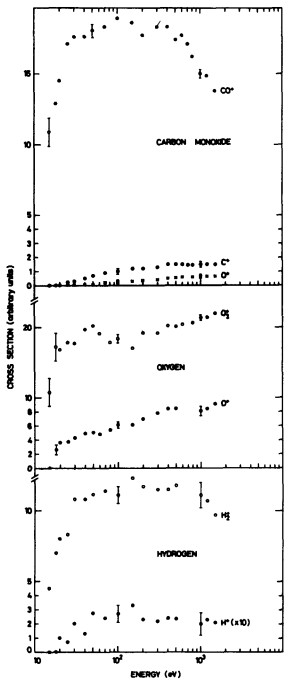

Fig. 5. — Chemi-ionization cross-sections of H_2, O_2 and CO by He metastable atoms as a function of relative energy. σ_{P+A} is shown by open circles, σ_D by closed circles. In the case of CO, the closed circles represent the dissociative ionization $\sigma_D(C^+)$ and the crosses the dissociative ionization $\sigma_D(O^+)$.

4.2.3 *Molecular oxygen.* — Product ions formed in the chemi-ionization of O_2 by He* have been measured between 15 and 1 500 eV. According to West *et al.* [29] the He* + O_2 system leads to the formation of a temporary excited molecule $(HeO_2)^*$, which preferentially autoionizes into the underlying HeO_2^+ continuum and dissociates into O_2^+. The electronic energies of He* + O_2 are higher than those of He + O_2^+ + e^- (Penning ionization) and He + O^+ + O + e^- (dissociative ionization) within the asymptotic limits of infinite interatomic separations (see Table I), so the processes He* + O_2 → He + O_2^+ + e^- and He* + O_2 → He + O^+ + O + e^- are exothermal. In accordance with this analysis O^+ production is considerable even for low energies (if we except the first experimental point at 15 eV, known within a 50 % uncertainty). The present results for a molecular oxygen target are shown on figure 5. The total ionization cross-section σ_{P+A} (open circles) exhibits a structure, increasing by 50 % from 15 to 18 eV then rising more slowly to reach a maximum near 60 eV followed by a well-resolved minimum around 100 eV. From 100 eV to 1 500 eV σ_{P+A} rises slowly. The total dissociative ionization cross-section σ_D (closed circles) increases slightly with energy over our whole experimental range ; a hint of structure is also observed in σ_D but is not interpreted at the present time.

In the thermal energy range Riola *et al.* [30] using a crossed beam technique, and Lindinger *et al.* [5] using a flowing afterglow, have measured the rate constants for the quenching of the $2\,^3S$ state of He by O_2. From these data the total chemi-ionization cross-section including all the various destruction channels is approximately 28 Å^2 for 0.1 eV relative energy. For the same reasons as those given for an H_2 target it is not possible to compare on an absolute scale the sets of data relevant to the thermal range and to the present energy range.

4.2.4 *Carbon monoxide,* — The total ionization cross-sections σ_{P+A} and σ_D for CO in collisions with He* are shown in figure 5. The closed circles represent the total chemi-ionization cross-section σ_{P+A} (exothermal case). For this heteronuclear target we have two endothermal dissociative ionization processes (see Table I) as shown in reactions 5 and 6, respectively :

$$He^* + CO \rightarrow$$
$$\rightarrow He + C^+ + O + e^- \quad \text{(closed circles)} \quad (19)$$

and

$$He^* + CO \rightarrow$$
$$\rightarrow He + C + O^+ + e^- \quad \text{(crosses)}. \quad (20)$$

The errors bars include statistical uncertainty on the data. σ_{P+A} rises sharply with energy from 15 to 30 eV then presents a quasi-plateau up to 600 eV with a slight maximum near 150 eV, decreasing afterwards with rising energy because of the exceedingly high relative velocity of the colliding partners. In the case of C^+ production σ_D presents a threshold at 20 eV then increases slowly with energy up to 500 eV, after which its value remains constant. The O^+ channel begins to rise in the neighbourhood of 30 eV then increases slowly with energy.

Comparing the two energy thresholds for reactions 19 and 20 we find that their respective positions agree qualitatively with the value of the energy defect for these reactions. In other words the energy threshold is all the higher as the reaction energy defect is large. Riola *et al.* [30] give an absolute value for the total chemi-ionization cross-section in the thermal energy range ; this value is approximately 23 Å (averaged for the singlet and triplet states) for a collision energy of 0.06 eV.

5. Conclusion.

The total chemi-ionization cross-sections reported here for each target gas colliding with metastable He atoms (He 2 ^{1}S and He 2 ^{3}S) include all processes which lead to the formation of slow target ions : Penning ionization giving rise to a slow ion from the autoionizing state $(HeX_2)^*$, excitation transfer followed by autoionization of the target $(X_2)^*$ which also gives a slow molecular ion, and dissociative ionization. We have neglected ionization caused by ground-state atoms in the He beam (see section 3.1). For N_2 and CO dissociative ionization processes and for the Ne ionization process the reactions have an energy defect of some eV and the slow ion flux becomes detectable above a relative energy threshold of a few tens of eV depending on the energy defect of the reaction. Associative ions are not observed under our experimental conditions because associative ionization corresponds to transitions with low relative kinetic energy, lower than the potential energy well of the associative state which is never the case in our experiments. To our knowledge no previous experimental or theoretical work exists for the target gases Ne, H_2, O_2 and CO at high energies. The measured Penning ionization and autoionization cross-sections for atomic and molecular target gases have been shown to be characterized by a strong energy dependence, excepting however the Ar target case where σ_{P+A} varies monotonically by 40 % along the energy range.

Concerning the endothermal reaction (Penning ionization and autoionization cross-section for Ne target, and dissociative ionization cross-section for N_2 and CO targets) the slow ion flux from these processes has been found to exhibit a threshold at a few tens of eV, showing that a relative kinetic energy varying from 16 to 44 eV (depending on the energy defect of the reaction) in the centre-of-mass coordinates is needed to transfer a few eV to the internal energy of the colliding system.

Acknowledgments.

The authors would like to thank Drs. A. Valance, G. Spiess and G. Watel for fruitful discussions.

References

[1] TANG, S. Y., MARCUS, A. B., MUSCHLITZ, E. E., *Chem. Phys.* **56** (1972) 556.
[2] PESNELLE, A., HOURDIN, A., WATEL, G., MANUS, C., *J. Phys. B* **6** (1973) L-326.
[3] PESNELLE, A., WATEL, G., MANUS, C., *J. Chem.* **62** (1975) 3590.
[4] ILLENBERGER, E., NIEHAUS, A., *Z. Physik B* **20** (1975) 33.
[5] LINDINGER, W., SCHMELTEKOPF, A. L., FEHSENFELD, F. C., *Chem. Phys.* **61** (1974) 2890.
[6] MIERS, R. E., SCHLACHTER, A. S., ANDERSON, L. W., *Phys. Rev.* **183** (1969) 213.
[7] GILBODY, H. B., BROWNING, R., REYNOLDS, R. M., RIDDEL, G. I., *J. Phys. B* **4** (1971) 94.
[8] PRADEL, P., ROUSSEL, F., SCHLACHTER, A. S., SPIESS, G., VALANCE, A., *Phys. Rev. A* **10** (1974) 797.
[9*a*] MORGENSTERN, R., LORENTS, D. C., PETERSON, J. R., OLSON, R. E., *Phys. Rev. A* **8** (1973) 2372.
[9*b*] GILLEN, K. T., PETERSON, J. R., OLSON, R. E., *Phys. Rev. A* **15** (1977) 527.
[9*c*] MOSELEY, J. T., PETERSON, J. R., LORENTS, D. C. HOLLSTEIN, M., *Phys. Rev. A* **6** (1972) 1025.
[10] NIEHAUS, A., in *The excited state in Chemical Physics*, part 2, edited by Mc Gowan, J. W., 1981, p. 399.
[11] LOCHT, R., SCHOPMAN, J., WANKENNE, H., MOMIGNY, J., *Chem. Phys.* **7** (1975) 393.
[12] LOCHT, R., *Chem. Phys.* **22** (1977) 13.
[13] DEHMER, P. M., CHUPKA, W. A., *J. Chem. Phys.* **62** 11 (1975) 4525.
[14] PRADEL, P., LAUCAGNE, J. J., *Chem. Phys. Lett.* **85** (1982) 48.
[15] PRADEL, P., EL MADDARSI, M., VALANCE, A., *J. Phys. B* **14** (1981) 541.
[16] SCHLACHTER, A. S., LOYD, D. H., BJORKHOLM, P. J., ANDERSON, L. W., HAEBERLI, W., *Phys. Rev.* **174** (1968) 201.
[17] HOLLSTEIN, M., SHERIDAN, J. R., PETERSON, J. R., LORENTS, D. C., *Phys. Rev.* **187** (1969) 118.
[18] REYNAUD, C., POMMIER, J., VU NGOC TUAN, BARAT, M., *Phys. Rev. Letters* **43** (1979) 579.
[19] PETERSON, J. R., LORENTS, D. C., *Phys. Rev.* **182** (1969) 152.
[20] BROWNING, R., GILBODY, H. B., *J. Phys. B* **1** (1968) 1149.
[21] HAGSTRUM, H. D., *Phys. Rev. Letters* **43** (1979) 1050.
[22] HULTGREN, R., DESAI, P. D., HAWKINS, D. T., GLEISER, M., KELLY, K. K., WAGMAN, D. D., *Selected values of the Thermodynamic Properties of the elements*, American Society for metals, 1973, p. 141.
[23] PRADEL, P., ROUSSEL, F., SPIESS, G., *Rev. Sci. Instrum.* **45** (1974) 49.
[24] COHEN, J. S., LANE, N. F., *J. Chem. Phys.* **66** (1977) 586.
[25] HICKMAN, A. P., ISAACSON, A. D., MILLER, W. H., *J. Chem. Phys.* **66** (1977) 1492.
[26] HOTOP, H., NIEHAUS, A., *Chem. Phys. Lett.* **3** (1969) 687.
[27] NEYNABER, R. H., MAGNUSON, G. D., *J. Chem. Phys.* **61** (1974) 749.
[28] SCHMELTEKOPH, A. L., FEHSENFELD, F. C., *J. Chem. Phys.* **53** (1970) 3173.
[29] WEST, W. P., COOK, T. B., DUNNING, F. B., RUNDEL, R. D., STEBBINGS, R. F., *J. Chem. Phys.* **60** (1974) 5126.
[30] RIOLA, J. P., HOWARD, J. J., RUNDEL, R. D., STEBBINGS, R. F., *J. Phys. B.* **7** (1974) 376.